Room-Temperature Isolation of V(benzene)$_2$ Sandwich Clusters via Soft-Landing into *n*-Alkanethiol Self-Assembled Monolayers

Shuhei Nagaoka,[†] Takeshi Matsumoto,[†] Eiji Okada,[†] Masaaki Mitsui,[†] and Atsushi Nakajima*[,†,‡]

Department of Chemistry, Faculty of Science and Technology, Keio University, 3-14-1 Hiyoshi, Kohoku-ku, Yokohama 223-8522, Japan, and CREST, Japan Science and Technology Agency (JST), c/o Department of Chemistry, Keio University, Yokohama 223-8522, Japan

Received: March 23, 2006; In Final Form: May 23, 2006

The adsorption state and thermal stability of V(benzene)$_2$ sandwich clusters soft-landed onto a self-assembled monolayer of different chain-length *n*-alkanethiols (C_n-SAM, $n = 8$, 12, 16, 18, and 22) were studied by means of infrared reflection absorption spectroscopy (IRAS) and temperature-programmed desorption (TPD). The IRAS measurement confirmed that V(benzene)$_2$ clusters are molecularly adsorbed and maintain a sandwich structure on all of the SAM substrates. In addition, the clusters supported on the SAM substrates are oriented with their molecular axes tilted 70−80° off the surface normal. An Arrhenius analysis of the TPD spectra reveals that the activation energy for the desorption of the supported clusters increases linearly with the chain length of the SAMs. For the longest chain C_{22}-SAM, the activation energy reaches ∼150 kJ/mol, and the thermal desorption of the supported clusters can be considerably suppressed near room temperature. The clear chain-length-dependent thermal stability of the supported clusters observed here can be explained well in terms of the cluster penetration into the SAM matrixes.

1. Introduction

Over the past decade, gas-phase synthesis by means of the laser vaporization of metals has provided various kinds of metal clusters as well as organometallic complexes. These gaseous clusters have generated a great deal of attention due to their strongly size-dependent properties that are often different from those of the bulk materials. In particular, since the discovery of the multidecked vanadium (V)− benzene sandwich complex V_n(benzene)$_{n+1}$,[1] a wide variety of experimental and theoretical efforts have been devoted to its characterization.[2−14] For example, it has been recently discovered that V_n(benzene)$_{n+1}$ clusters possess unique, size-dependent electronic[10−12] and ferromagnetic[13,14] properties originating from their 1D structures. Hence, they are expected to become one of the most promising candidates for use as building blocks in nanodevices.

Nondissociative deposition of mass-selected cluster ions produced in the gas phase onto a pertinent substrate, a so-called "soft-landing", provides a possible use for the intriguing clusters as building blocks in cluster-based nanomaterials. Recently, surface modification via soft-landing of gas-phase ionic compounds such as metal clusters and biomolecules onto a solid surface increasingly enables the creation of new types of nanoscale materials, e.g. nanocatalysts,[15−17] nanomagnetics,[18−20] and biological microarrays.[21−23] However, there are rather few studies of soft-landing or vapor deposition of the organometallic sandwich complexes onto solid surfaces. In our laboratory, V(benzene)$_2$ sandwich clusters have been soft-landed onto a gold substrate covered with a low-temperature Ar matrix, and infrared spectroscopy has confirmed that they adopt a sandwich structure.[24] While direct deposition of the gaseous clusters onto a bare metal surface often results in dissociation of the clusters upon impact, the rare gas matrix can serve as a buffer layer, dissipating the kinetic energy of the projectile clusters and keeping the cluster largely intact.[25,26] However, the use of the rare gas matrix is limited to extremely low substrate-temperature conditions, because the rare gas Ar matrix evaporates at a temperature of ∼18 K.

After soft-landing, the clusters inevitably undergo an interaction with a substrate surface. A profound insight into the cluster−surface interaction is critical for the fabrication of cluster-based nanomaterials. A study of the catalyzed oxidation of CO on Au_8 clusters soft-landed on a magnesia surface, for instance, demonstrated that a charging of the metal cluster, caused by the partial transfer of charge from an F-center of the surface into the deposited cluster, underlies the catalytic activity of the Au_8 clusters.[17] The F-centers further serve to strongly anchor the deposited clusters, thereby inhibiting their diffusion and coalescence on the surface until temperatures of ∼350 K.

On a related note, the adsorption properties of 1D organometallic sandwich complexes on metal surfaces have been studied by physical vapor deposition onto the surface under ultrahigh vacuum (UHV) conditions.[27−29] In strong contrast to the supported metal clusters, organometallic clusters are considered to be rather unstable with respect to bare metal surfaces. Indeed, Blass et al. demonstrated that a Cr(benzene)$_2$ sandwich complex chemisorbed on a Ni(100) surface dissociates its ligand−metal bond due to a strong perturbation from the Ni(100) surface.[28] Thus, to support organometallic complexes on a substrate, the use of a chemically inert substrate is required to reduce such metal surface perturbations. However, a study of the adsorption of ferrocene, Fe(C_5H_5)$_2$, on a relatively inert Ag(100) surface showed that ferrocene adsorbs molecularly on an Ag(100) surface, but the weak adsorbate−surface interaction

* To whom correspondence should be addressed. E-mail: nakajima@chem.keio.ac.jp. Fax: +81-45-566-1697.
† Keio University.
‡ Japan Science and Technology Agency (JST).

10.1021/jp061806+ CCC: $33.50
Published on Web 07/21/2006

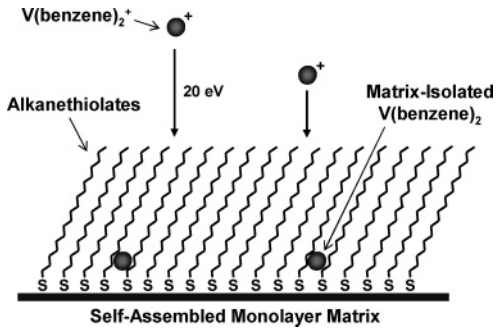

Figure 1. Schematic illustration of the soft-landing isolation of gas-phase synthesized V(benzene)$_2$ cations into an *n*-alkanethiol self-assembled monolayer (SAM) matrix where the alkyl chains are densely packed and tilted ~30° with respect to the surface normal. The incoming cluster cations with high incident energy of 20 eV penetrate into the SAM matrix and are neutralized by charge transfer from the substrate. The structural disordering in the alkanethiolates induced by collisions with the cluster ions and capturing of the penetrated clusters is not shown here.

permits the thermal desorption of the adsorbed ferrocene at temperatures as low as 200 K. This desorption occurs because of the small desorption activation energy (or adsorption heat).[29] Therefore, an ingenious cluster-supporting methodology, realizing both a small structural perturbation (i.e. maintenance of the sandwich structure) and a high adsorption heat (i.e. a high desorption temperature) of the supported organometallic sandwich clusters, is a highly desired goal.

Recently, Cooks and co-workers have described a technique to support gas-phase ionic species on a solid surface.[30−32] They have achieved trapping of gas-phase polyatomic ions using a self-assembled monolayer (SAM) of fluorocarbon as the supporting matrix.[30] They have also shown that the soft-landed bulky polyatomic ions can penetrate into the SAM and they are sterically trapped inside the SAM, while retaining their charge. Another important ability of the SAM has been demonstrated, in that it can serve as a effective buffer layer like a rare gas matrix, dissipating the kinetic energy of the projectiles.[33−35] For example, Day et al. have performed a detailed study of a rare gas collision with *n*-alkanethiolate SAMs and found that the long-chain alkanethiolate SAM effectively dissipates the translational energy of the projectile atom.[33] They estimated that more than 80% of the incident energy of the projectiles transferred to the internal energy of the organic surface. On the basis of the above-mentioned results, SAMs are likely to be promising matrixes to suppress the dissociation of the clusters in the soft-landing process and to realize the effective trapping of intact clusters.

Toward this ambitious end, we have recently used long-chain alkanethiolate-SAMs as cluster-trapping matrixes and succeeded in the room-temperature matrix isolation of the gas-phase synthesized vanadium−benzene 1:2 sandwich clusters, V(benzene)$_2$, in the *neutral* state.[36] The SAM matrix-isolation scheme of the gas-phase clusters via soft-landing is shown in Figure 1. In this article, we present a full account of our experimental results obtained for the alkanethiolate-SAM matrix isolation of the V(benzene)$_2$ sandwich clusters via a soft-landing technique. The V(benzene)$_2$ clusters produced in the gas phase were size-selectively soft-landed onto a bare gold substrate and on various chain-length *n*-alkanethiolate self-assembled monolayers (C_n-SAM with $n = 8$, 12, 16, 18, and 22). The adsorption state and thermal chemistry of the soft-landed clusters were examined by means of infrared reflection absorption spectroscopy (IRAS) and temperature-programmed desorption (TPD). A highly oriented adsorption geometry as well as an unusually large adsorption heat of the adsorbed sandwich clusters was confirmed for the long-chain C_n-SAM substrates through the analysis of the IRAS and TPD results obtained. Further clarification of the origin of these findings was attempted by an examination of the chain-length effect of the alkanethiolate-SAM matrix on the thermal chemistry of the soft-landed clusters. Consequently, it is confirmed that both the orientational preference and the high thermal stability of the clusters are due to the cluster penetration into the SAM matrix.

2. Experimental Section

2.1. Substrate Preparation. A commercially available 10 × 10 mm^2 gold substrate, Au(100 nm thickness)/Ti/Silica (Auro Sheet, Tanaka Precious Metals Co. Ltd.) having ~50 nm grains, was used as a gold surface. To remove organic contaminants from the gold surface, the substrate was chemically cleaned by dipping in a piranha solution (3:1 concentrated H_2SO_4−H_2O_2)[37,38] for about 20 min. A series of alkanethiolate-SAM (C_n-SAM: $n = 8$, 12, 16, 18, and 22) substrates was prepared by immersing the gold substrates into a 2 mM ethanolic solution of various alkanethiols of octanethiol ($C_8H_{17}SH$), dodecanethiol ($C_{12}H_{25}SH$), hexadecanethiol ($C_{16}H_{33}SH$), octadecanethiol ($C_{18}H_{37}SH$), and docosanethiol ($C_{22}H_{45}SH$) at ambient temperature for 20 h. The formation of the SAM on the gold substrate was confirmed by IRAS and contact angle measurements (Drop Master 300, Kyowa Interface Science) at room temperature.

2.2. Soft-Landing Experiments. The details of the soft-landing apparatus have been described elsewhere.[24] Briefly, it consists of a cluster source, ion optics, a mass selection stage, and a deposition chamber where TPD and IRAS experiments are performed. A reaction between laser-vaporized vanadium (V) atoms and benzene vapors produced V−benzene sandwich clusters in the expansion from a piezo-driven pulsed valve under a helium stagnation pressure of ~4 atm. The cluster cations thus produced were guided into the deposition chamber by a series of ion optics, i.e., octapole ion guides, a quadrupole deflector, and electrostatic lenses. Only the V(benzene)$_2^+$ clusters were size-selected ($m/z = 207$) by a quadupole mass filter (4−4000 amu, Extrel); subsequently, the cluster cations were deposited onto a substrate with a collision energy of 20 ± 10 eV under UHV conditions (~2 × 10^{-10} Torr). The substrate could be cooled to ~120 K by contact with a liquid-nitrogen reservoir, and the substrate temperature was kept at ~180 K during the deposition by means of a heating element. The total amount of the deposited cluster ions was determined by integrating the ion current on the substrate during the cluster deposition.

2.3. IRAS Measurements. The IRAS measurements were performed with a FT-IR spectrometer (IFS 66v/S, Bruker): a collimated IR beam emerging through one of the side ports of the spectrometer was focused onto the sample substrate at a grazing incidence angle of ~80° from the surface normal through a flat KBr window. After the reflection from the substrate, the IR beam exiting through another KBr window at the opposite side of the apparatus was directed onto an off-axis parabolic mirror, which refocused the beam onto the active element of a liquid-nitrogen-cooled mercury cadmium telluride (MCT) detector. The IR optics and the detector were mounted in a vacuum chamber pumped to a pressure of about 0.1 Torr to remove spectral background contributions due to atmospheric gases, mostly carbon dioxide and water vapor. All spectra were recorded with a spectral resolution of 2 cm^{-1}. A total of 500 scans were accumulated for the background and sample spectra, which were recorded before and after the cluster deposition,

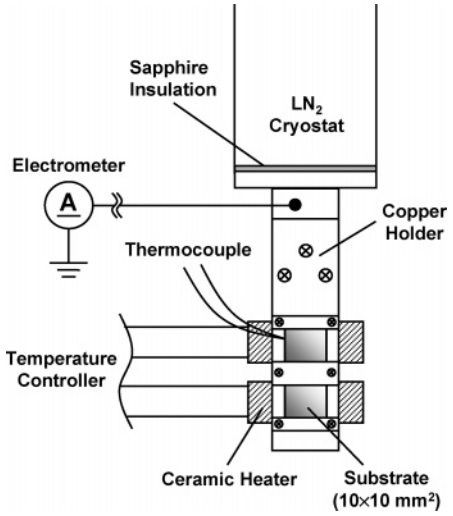

Figure 2. Details of the sample holder in the deposition chamber. To cool the substrates efficiently using a LN_2 reservoir, a high thermal conductivity material (copper) was used for the sample holder. The ceramic heaters mounted inside the holder were placed in mechanical contact with the substrates to provide rapid and even heating. The surface temperature was measured by a type-K chromel−alumel thermocouple and controlled by a proportional integral differential (PID) operation programmed by a temperature controller unit.

TABLE 1: Contact Angle of Water Drops (1 μL) on the *n*-Alkanethiol SAMs and the Gold Substrate

substrate	contact angle (deg)
C_8-SAM	104 ± 1
C_{12}-SAM	107 ± 1
C_{16}-SAM	105 ± 1
C_{18}-SAM	106 ± 2
C_{22}-SAM	107 ± 1
bare gold	∼0

respectively. The data acquisition was performed with Bruker OPUS software.

2.4. TPD Measurements. The thermal desorption of the deposited clusters was induced by heating the substrate with a ceramic heater (MS-1, Sakaguchi E.H Voc Corp.) that was directly attached to it, as shown in Figure 2. The surface temperature was monitored by a type-K thermocouple, and the heating rate, controlled by a temperature controller unit (SDR-S30-P, Sakaguchi E.H Voc Corp.), was typically set at ∼1 K/s. The desorbed clusters were ionized by electron impact and then detected by a quadrupole mass spectrometer (4−4000 amu; 150-QC, Extrel). The entrance of the mass spectrometer was restricted by a stainless steel skimmer (5 mm i.d., placed ∼1 mm above the substrate) to detect only the species desorbed from the substrate surface.

3. Results and Analysis

3.1. Characterization of SAM Substrates. The contact angles of a water droplet (1 μL) on the bare gold and C_n-SAM-coated gold substrates (n = 8, 12, 16, 18, and 22) that were used in the current soft-landing experiment are listed in Table 1. While the bare gold surface was completely wetted (∼0°), the hydrophobic nature of all the C_n-SAMs examined was revealed by their large contact angles of 100−110°. The contact angles obtained are in good agreement with literature values for the corresponding C_n-SAMs anchored on gold surfaces.[39,40]

Figure 3 shows the C−H stretching region of the IRAS spectra for the above C_n-SAMs; these data are in good accordance with previously reported IRAS spectra.[41,42] Thus,

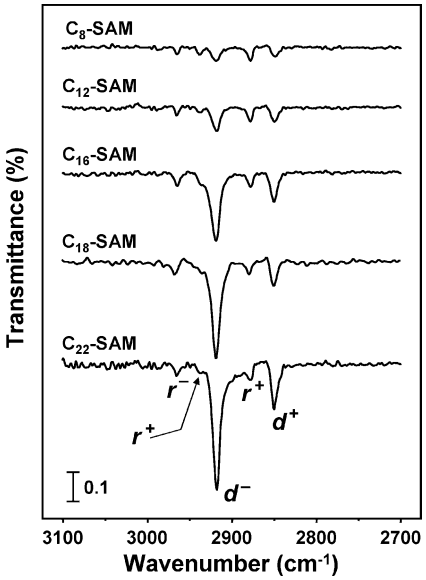

Figure 3. IRAS spectra in the C−H stretching region (2700−3100 cm^{-1}) for *n*-alkanethiols adsorbed on the gold substrate measured at room temperature.

the bands denoted as r^+ and r^- can be assigned to the antisymmetric and symmetric stretching modes of the terminal methyl group, respectively. The r^+ peak is split into a doublet, because of Fermi resonance interactions with the overtone of the lower frequency methylene scissoring mode.[43,44] The d^+ and d^- peaks, whose intensities increase with the alkyl-chain length, are respectively assigned to the antisymmetric and symmetric methylene stretching modes. The observed vibrational frequencies of the methylene modes (d^+ and d^-) in the long-chain C_{16}- to C_{22}-SAMs agree with those of crystalline-state alkanethiolate-SAMs, indicating the formation of densely packed, crystallike alkanethiolate monolayers on the gold surfaces. In the short-chain C_8- and C_{12}-SAM spectra, the d^- peak is slightly shifted toward higher frequency (2920 cm^{-1}), a change which is probably due to a partial disordering of the short-chain C_8- and C_{12}-SAMs at room temperature.[41]

3.2. IRAS Spectra of V(benzene)$_2$ Clusters. The IRAS spectra in the 700−1500 cm^{-1} region of V(benzene)$_2$ clusters soft-landed on (a) bare gold and (b) C_{18}-SAM substrates at 180 K are shown in Figure 4 as a function of the deposition number of the cluster cations. The deposition of 2.0×10^{14} V(benzene)$_2$ cation/cm^2 seemingly provides an approximate monolayer coverage (i.e. 1 ML). However, the deposition process may be accompanied by recoiling and/or dissociation of the cluster ions in the collision with the substrate surface, so that the deposition numbers presented here correspond to the *apparent* upper limits of the amounts of nondestructively deposited, i.e., "soft-landed", clusters. As shown in Figure 4a, two adsorption bands at 956 and 988 cm^{-1} start to appear when approximately 1.0×10^{14} cations have been deposited onto the bare gold substrate. In the deposition-number range of $\geq 4.0 \times 10^{14}$ ions, an additional two bands appear at 747 and 1418 cm^{-1}. In contrast, with a C_{18}-SAM substrate, these four bands can be clearly observed at a much lower deposition number (i.e. $< 1.0 \times 10^{14}$), suggesting that this substrate permits a rather higher soft-landing efficiency than does the bare gold. The four bands observed for each substrate are in good agreement with the fundamentals reported in IR data for a *neutral* V(benzene)$_2$ complex in an Ar matrix.[8,45] Thus, we can assign the bands as follows: that at 747 cm^{-1} to a C−H out-of-plane bending [ν_{o-p}(CH)], that at 956 cm^{-1} to a symmetric ring-breathing mode [ν_s(CC)], that at

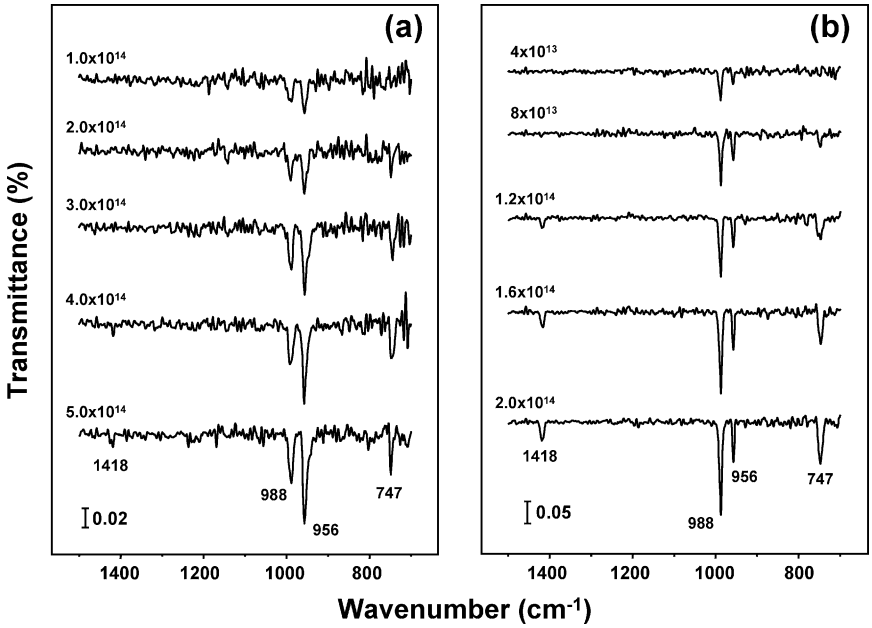

Figure 4. IRAS spectra in the 700−1500 cm^{-1} region for the V(benzene)$_2$ clusters at several deposition numbers on (a) gold and (b) C_{18}-SAM at 180 K.

988 cm^{-1} to the C−H in-plane bending mode [ν_{i-p}(CH)], and that at 1418 cm^{-1} to the asymmetric C−C stretching mode [ν_a-(CC)]. These agreements indicate that the soft-landed V(benzene)$_2$ cluster cations lose their charge, and the resulting neutral clusters adsorb on both the substrates with their native sandwich structure intact.

However, the relative intensities of the four bands differ strikingly in the V(benzene)$_2$/gold and the V(benzene)$_2$/C_{18}-SAM spectra. In particular, the band intensity ratio of 956 to 988 cm^{-1} in the V(benzene)$_2$/gold spectrum completely reverses in the V(benzene)$_2$/C_{18}-SAM spectrum. Similar spectral feature intensities have also been identified for the other C_n-SAM substrates (n = 8, 12, 16, and 22).[36] Due to the surface selection rule of IRAS,[46] the relative absorption intensity qualitatively reflects the orientation of an adsorbate on a surface. Thus, the remarkable difference in the relative peak intensities suggests that the adsorption geometry of the clusters on the SAM substrate is different from that on the bare gold.

3.3. Estimation of Orientation Angle of V(benzene)$_2$ Clusters on SAM Substrates. The V(benzene)$_2$ sandwich cluster ideally belongs to the D_{6h} point group, and it can thereby possess two IR-active A_{2u} and E_{1u} symmetry vibrational modes. In fact, the four IR peaks observed herein are due to two A_{2u} modes (747 and 956 cm^{-1}) and two E_{1u} modes (988 and 1418 cm^{-1}). The vibrational modes with A_{2u} symmetry give rise to transition dipoles along the D_{6h} symmetry molecular axis of the V(benzene)$_2$ cluster (i.e. along the benzene−V−benzene direction). In contrast, the modes with E_{1u} symmetry arise from dipoles oriented perpendicular to the molecular axis. Owing to the IRAS surface selection rule, only vibrational modes whose transition dipole is perpendicular to the surface are potentially observable in the spectrum. Hence, when the V(benzene)$_2$ cluster adsorbs with its molecular axis perpendicular to the surface, only the A_{2u} modes are expected to be dipole active. At the other extreme, when the cluster adsorbs with the molecular axis parallel to the surface, only the E_{1u} modes are observable. In the case of the gold substrate, the IR peak intensity distribution of the A_{2u} and E_{1u} modes is quite similar to that of the V(benzene)$_2$/Ar matrix spectrum (see Figure 4a). As the V(benzene)$_2$ clusters isolated in an Ar matrix are randomly oriented in space, the result suggests that the V(benzene)$_2$ clusters are adsorbed with random orientations on the gold surface. For the C_{18}-SAM substrate, however, a dramatic change is found in the relative IR peak intensity: namely, the two E_{1u} modes at 988 and 1418 cm^{-1} become rather more intense than the two A_{2u} modes at 747 and 957 cm^{-1}. Therefore, it can be expected that the V(benzene)$_2$ clusters that soft-landed onto the C_{18}-SAM substrate are highly oriented, and that their molecular axis is tilted substantially off the surface normal.

TABLE 2: Orientation Angle (Θ, deg) and Adsorption Heat (E_d, kJ/mol) of the V(benzene)$_2$ Clusters Soft-Landed on Each Substrate

substrate	Θ	E_d
bare gold		64 ± 13
C_8-SAM	69 ± 2	90 ± 19
C_{12}-SAM	71 ± 1	110 ± 26
C_{16}-SAM	73 ± 2	130 ± 10
C_{18}-SAM	72 ± 1	138 ± 21
C_{22}-SAM	78 ± 6	153 ± 27

The orientation angle of an adsorbate can be semiquantitatively determined by the RATIO method.[47] With the assumption that all the soft-landed V(benzene)$_2$ clusters are oriented uniformly on the substrate, the *averaged* tilt angle (Θ) of the clusters with respect to the surface normal is given by comparing the intensity ratio of the A_{2u} and E_{1u} modes as follows:[36]

$$\sin^2 \Theta = 2/\{2 + [I^{SAM}(A_{2u})/I^{SAM}(E_{1u})]/[I^{Ar}(A_{2u})/I^{Ar}(E_{1u})]\} \quad (1)$$

Here I^{SAM} represents the IR absorption intensity in the oriented state (i.e. the SAM substrate) and I^{Ar} indicates the corresponding intensity in the random orientation (i.e. the Ar matrix). The analytical results, summarized in Table 2, demonstrate the large orientation angles (Θ = 70−80°) of the soft-landed V(benzene)$_2$ clusters on all the SAM substrates examined.

3.4. Evaluation of Thermal Stability of V(benzene)$_2$ Clusters via IRAS Measurements. To gain insight into the thermal stability of the soft-landed V(benzene)$_2$ clusters on each substrate, we examined the temperature-induced variations of the IRAS spectra, shown in Figure 5. The upper traces in Figure 5a,b depict the IR spectra of the V(benzene)$_2$ clusters on the

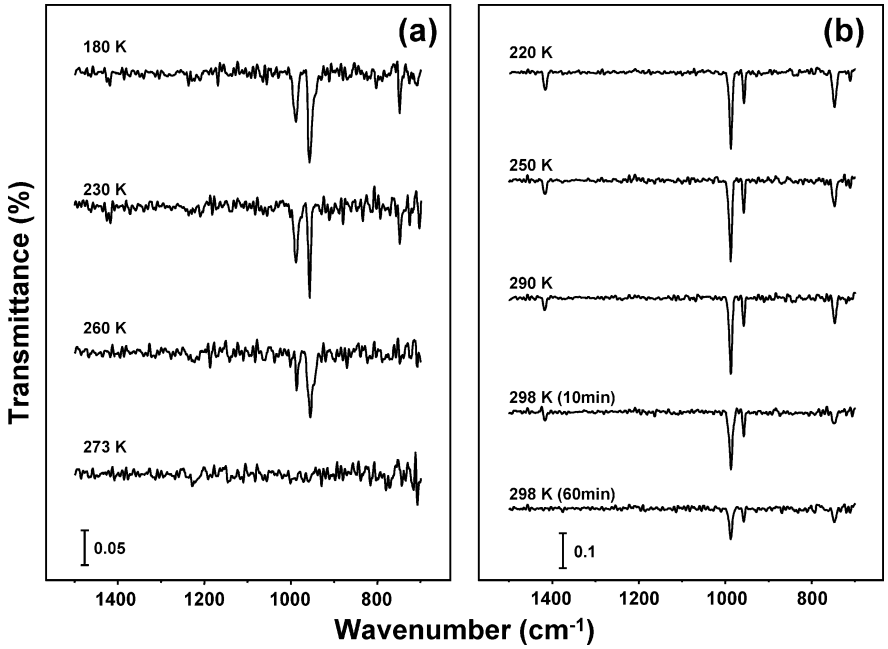

Figure 5. IRAS spectra showing the temperature-dependent variation of the V(benzene)$_2$ clusters after deposition of (a) 5.0×10^{14} ions onto gold and (b) 2.0×10^{14} ions onto C_{18}-SAM at 180 K.

bare gold and C_{18}-SAM substrates at 180 K taken after depositions of 5.0×10^{14} and 2.0×10^{14} cations, respectively. In the case of the gold substrate, the intensity reduction begins to occur around 230 K, and the bands completely vanish at 273 K (0 °C). In contrast, all the peaks in the V(benzene)$_2$/C_{18}-SAM spectra do not decrease in intensity up to 290 K, but they start to decrease very slowly at 298 K (25 °C). After the substrate temperature is kept at 298 K for 1 h, the bands at 747, 956, and 988 cm^{-1} are still observed in the spectrum, although the intensities decrease to about 40% of their initial intensities. Note that once the peak intensities have decreased due to substrate heating, they never return to their initial values, even if the substrate is cooled again to the initial temperature (180 K). This irreversibility can be reasonably explained by thermal desorption of the adsorbed clusters from the substrates, because the decrement of the IR band intensity starts at the same temperature as the desorption threshold temperature for the TPD spectrum. Below, we show that the desorption temperature of the adsorbed V(benzene)$_2$ clusters on the C_{18}-SAM substrate is approximately 70 K higher than that on the gold substrate. Although the IRAS spectra clearly indicate the physisorption of the V(benzene)$_2$ clusters on both of the substrates, this result interestingly suggests that the activation energy for the desorption (i.e. adsorption heat) of the adsorbed clusters is much different between these two substrates.

Figure 6 shows the substrate-temperature effect on the orientation angles of the supported clusters on the short-chain C_8-SAM and the long-chain C_{18}-SAM. For the long-chain C_{18}-SAM, the average orientation angle of the clusters barely changes (within ±0.5°) below the threshold desorption temperature of ~300 K, a result indicating no change in the adsorption geometry of the clusters remaining on the C_{18}-SAM substrate. In contrast, the average orientation angles for the clusters supported on the short-chain C_8-SAM alter by ±3°, depending on the surface temperature. As will be discussed later, this fluctuation is attributed to the reduced rigidity of the short-chain SAMs.

3.5. TPD Spectra of V(benzene)$_2$ Clusters. In the TPD measurements, the deposition number of the cluster ions was set to provide a relatively low coverage of ≤0.2 ML (i.e. 4.0×10^{13} ions/cm^2) so that aggregations and interactions between the adsorbed clusters themselves on the substrate might be reduced. Figure 7 shows typical TPD spectra for the V(benzene)$_2$ clusters on the gold and the C_{18}-SAM substrates. The desorbed species detected consisted mainly of three kinds of ions:

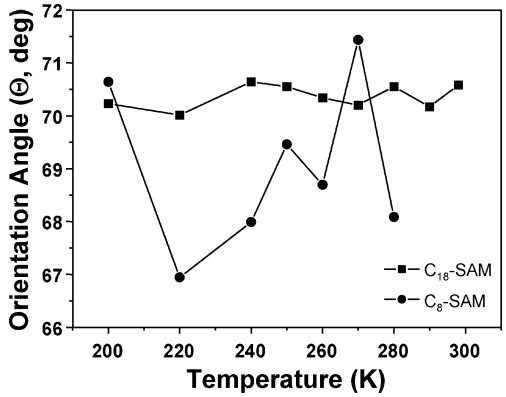

Figure 6. Temperature dependence of the average orientation angle of the V(benzene)$_2$ clusters soft-landed on (●) C_8-SAM and (■) C_{18}-SAM at 200 K.

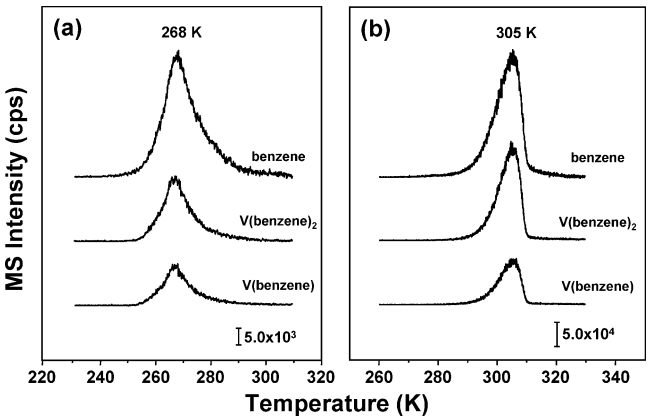

Figure 7. Multiplexed thermal desorption data for the V(benzene)$_2$ clusters soft-landed on (a) gold and (b) C_{18}-SAM after deposition of 4×10^{13} cluster ions at 180 K.

V(benzene)$_2^+$ ($m/z = 207$); V(benzene)$_1^+$ ($m/z = 129$); benzene$^+$ ($m/z = 78$). It should be noted that these ion signals were not observed in the absence of electron impact ionization in the mass spectrometer, a result explicitly confirming that the soft-landed cluster ions are neutralized on the substrates. In the TPD spectra for each substrate, all of the three ions exhibit identical peak shapes; the temperatures of the threshold and maximum desorption are the same. The close similarity between the peak shapes of parent and fragmented species shows that these ions were obtained from a unique ionization process of *neutral* V(benzene)$_2$. Thus, the V(benzene)$_1^+$ and benzene$^+$ ions are produced *not* on the surface but in the electron impact ionization event of the parent V(benzene)$_2$ cluster in the mass spectrometer. For the bare gold substrate, as shown in Figure 7a, the desorption of the V(benzene)$_2$ clusters starts at ~240 K (i.e. a threshold desorption temperature) and the desorption rate reaches a maximum at ~270 K. The TPD curves display a nearly symmetric shape in which the ion intensity slowly decreases after the peak maximum. In the case of the C_{18}-SAM, however, the desorption temperature and the shape of the TPD curves differ greatly from those of the gold substrate, as shown in Figure 7b. In good agreement with the IRAS study mentioned in section 3.4, the threshold desorption temperature of the clusters on the C_{18}-SAM substrate is higher than that on the gold, a finding indicating that the soft-landed clusters are more strongly bound on the C_{18}-SAM substrate than on the gold substrate. Furthermore, the TPD curve for the V(benzene)$_2$/C_{18}-SAM substrate exhibits a sharp decrease after the peak maximum. In general, a peak profile of a TPD spectrum reflects the reaction order of a desorption process.[48,49] Thus, the peak shape difference observed herein suggests that the desorption process of the V(benzene)$_2$ clusters is significantly different between the gold and the C_{18}-SAM substrates. In addition, the integrated areas of the V(benzene)$_2$ TPD spectra, corresponding to the amount of V(benzene)$_2$ clusters deposited intact, are much larger for the C_{18}-SAM than for the gold substrate. The integrated areas of the V(benzene)$_2^+$ peak in the V(benzene)$_2$/C_{16-22}-SAM spectra are typically about 10 times larger than that for the gold substrate. As mentioned in section 3.2, this result also shows that the SAM matrix can behave as a buffer layer to efficiently reduce the recoils and/or decomposition of the incoming cluster ions in the landing process.

The effect of the SAM chain length on the thermal chemistry of the soft-landed V(benzene)$_2$ clusters was systematically studied by means of TPD measurements. Displayed in Figure 8 are TPD spectra for V(benzene)$_2$ clusters desorbed from C_n-SAM (with $n = 8$, 12, 16, 18, and 22) after deposition of 4.0×10^{13} cations of the clusters onto each substrate. For comparison, the TPD spectrum of V(benzene)$_2$/gold is also shown as the upper trace. The threshold desorption temperatures of the clusters on all the SAM substrates are higher than that for the bare gold substrate, and they gradually increase with the chain length of the SAM. This result demonstrates that the soft-landed clusters are more strongly trapped by longer chain SAMs. In addition, the peak shape of the V(benzene)$_2^+$ signal systematically varies with the chain length of the SAM. Although an asymmetric shape is observed for the long-chain C_{16-22}-SAMs, a tail at the high-temperature side of the peak tends to be observed in the V(benzene)$_2$/C_8- and C_{12}-SAM spectra. As discussed later, these results are closely related to the rigidities of the densely packed SAMs.

3.6. Arrhenius Analysis of TPD Spectra. The reaction order and activation energy for the desorption (adsorption heat) of adsorbed clusters can be evaluated through an analysis of their

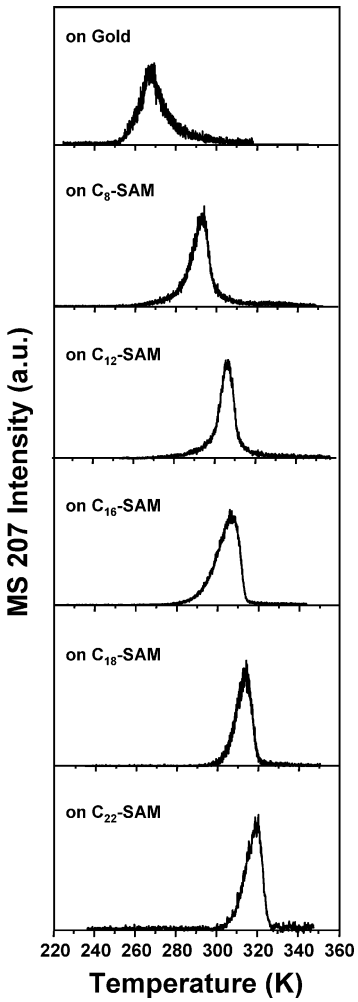

Figure 8. Temperature-programmed desorption spectra obtained for the V(benzene)$_2$ ($m/z = 207$) clusters soft-landed on the C_8- to C_{22}-SAMs, together with the gold substrate after deposition of 4×10^{13} cluster ions at 180 K.

TPD profiles. On a solid surface, the desorption rate equation (the Polanyi−Wigner equation) of adsorbates is given by

$$\ln k_d = \ln\left[\left(-\frac{d\theta}{dt}\right)/\theta^n\right] = \ln \nu_d - \frac{E_d}{RT} \qquad (2)$$

where k_d is the desorption rate constant, θ is the coverage, n is the reaction order, ν_d is a preexponential factor, and E_d is the adsorption heat.[50] The observed TPD profile provides the desorption rate ($-d\theta/dt$) and the coverage (θ), so that if a correct reaction order value, n, is chosen, a plot of ln k_d versus $1/T$ (i.e. an Arrhenius plot) should be linear. However, when an incorrect value of reaction order, m, is substituted, the expression possesses an additional term containing θ, as in the following:[48]

$$\ln\left[\left(-\frac{d\theta}{dt}\right)/\theta^m\right] = \ln \nu_d - \frac{E_d}{RT} + (n - m)\ln \theta \qquad (3)$$

This Arrhenius plot does not retain its linearity because θ is not linear with respect to $1/T$. In this analysis, four different reaction order values ($n = 0$, 0.5, 1, and 2) were examined to find the correct reaction order, n.

Figure 9 shows the Arrhenius plots for the TPD spectra of the V(benzene)$_2$ clusters desorbed from the bare gold, C_8-SAM, and C_{18}-SAM substrates. Linear plots were obtained only for a

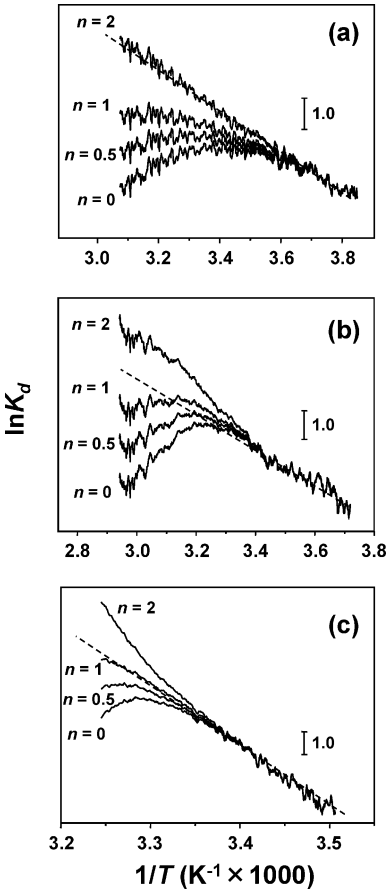

Figure 9. Arrhenius plots based on eq 2 from the TPD spectra of the V(benzene)$_2$ clusters obtained for (a) gold surface, (b) C_8-SAM, and (c) C_{18}-SAM with reaction orders of $n = 0$, 0.5, 1, and 2. The reaction orders were obtained by the best linear fit (the dotted line) to the plot of $n = 2$ for the gold and $n = 1$ for C_{18}-SAM, but a linear plot could not be obtained for the C_8-SAM for all values of n.

reaction order of $n = 2$ for the gold substrate (Figure 9a) and $n = 1$ for the C_{18}-SAMs (Figure 9c), while the plots obtained using other values were nonlinear in the high-temperature range (i.e. small $1/T$). The slope of the linear fit yielded a value of 64 $\pm$ 13 kJ/mol for the adsorption heat of the clusters on the bare gold. In the case of the C_{18}-SAM, the adsorption heat was determined to be 138 $\pm$ 21 kJ/mol, comparable to the typical adsorption heat of chemisorption ($\sim$100 kJ/mol). For the long-chain C_{16}- and C_{22}-SAMs, linear plots were also obtained with a reaction order of $n = 1$, just as for the C_{18}-SAM. As shown in Figure 9b, however, a linear plot could not be obtained for any value of n for the shorter chain C_8- and C_{12}-SAMs, a finding indicating that the desorption rate does not necessarily follow the simple desorption model of the Polanyi−Wigner equation (eq 2). Thus, in the case of the C_8- and C_{12}-SAMs, the adsorption heats were determined from the slope of the relatively large $1/T$ region where the plot is approximately linear and has the same slope for all choices of n.[51] The adsorption heats (E_d) thus obtained are also listed in Table 2, and plotted against the length of the SAM in Figure 10. Interestingly, the E_d value almost linearly increases with the chain length of the SAM.

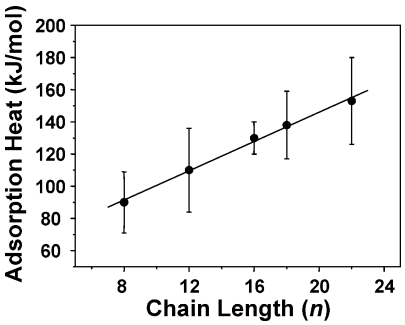

Figure 10. Apparent adsorption heat of the V(benzene)$_2$ clusters soft-landed on the SAMs plotted against the chain length of the SAM (●). The adsorption heat was obtained by a slope of the linear Arrhenius plot with a reaction order of $n = 1$ for C_{16}- to C_{22}-SAM and $n = 2$ for the bare gold. For the shorter chain C_8- and C_{12}-SAM, the adsorption heats were extracted by threshold temperature programmed desorption (TTPD) analysis in which linear plots were obtained independently of the value of n. The solid line was provided by least-squares fitting of the data (●).

4. Discussion

The IRAS results confirmed that V(benzene)$_2$ clusters are nondissociatively adsorbed on both the gold and SAM substrates, and retain the D_{6h} sandwich structure. On each substrate, furthermore, the IR absorption frequencies of the soft-landed V(benzene)$_2$ cations are in good agreement with those of their *neutral* cluster[8,45] but are different from those of the cation in gas-phase,[5] results indicating that the V(benzene)$_2$ cations are neutralized in the landing process by electron transfer from the substrates. Indeed, the average ion currents during the cluster cation deposition did not change between those for the gold and for the alkanethiolate-SAM substrates. It has been reported that a highly polar, fluorinated SAM can suppress the neutralization of projectile ions at the surface and trap the deposited ion intact;[30−32,52] however, such an effect is unlikely for the alkanethiolate-SAMs.

On an Au(111) surface at low temperature, the previous IRAS study revealed that a benzene molecule preferentially adsorbs in a "flat-lying" geometry with the molecular plane parallel to the surface plane due to interactions of the benzene π orbitals with the gold surface.[53] Thus, the V(benzene)$_2$ clusters might also prefer to adsorb via the flat-lying geometry where the capping benzene rings of the cluster are parallel to the gold surface. When the V(benzene)$_2$ adsorbs in this manner, only the A_{2u} modes at 747 and 956 cm^{-1} should be IR active on the gold surface, because of the surface selection rule. Furthermore, the bonding interaction of the benzene π orbitals with the gold surface should lead to a frequency shift of the vibrational modes of the benzene ring. Indeed, the frequency of the ν_{o-p}(CH) mode of benzene adsorbed on a Au(111) surface in this geometry is shifted more than 10 cm^{-1} to higher frequency than that of free benzene.[53] However, the V(benzene)$_2$/gold IRAS spectra observed herein clearly display both the A_{2u} modes at 747 and 956 cm^{-1} and the E_{1u} modes at 988 and 1418 cm^{-1} with the remaining vibrational frequencies corresponding to those of the condensed-phase observed in an Ar matrix.

This finding suggests that the clusters adsorb in random orientations on the gold surface, possibly because of facile surface diffusion of the adsorbed clusters. The surface diffusion of adsorbates has often been observed on a metal surface, because the potential barrier for the lateral motion of adsorbates on a metal surface is usually small enough to permit diffusion, except at extremely low temperatures.[54,55] Hence, the clusters diffuse on the surface as two-dimensional gases and can form islands of the clusters at step and defect sites existing on the gold surface at the relatively high surface temperature of 180 K. Such adsorption states exhibit an apparently random orientation on the surface and generate the IR bands of both the A_{2u} and E_{1u} vibrational modes in the IRAS spectra. Consequently, the IRAS spectra for the V(benzene)$_2$/gold are identical with

the IR spectra of V(benzene)$_2$ in an Ar matrix where the clusters are randomly oriented in space.

The thermal desorption studies also support the occurrence of surface diffusion of the clusters on the surface. As noted above, the desorption of the adsorbed V(benzene)$_2$/gold clusters is second-order. Although second-order desorption kinetics is often characterized by a recombination desorption of dissociatively adsorbed molecules,[46,50,51] the IRAS study shows that the soft-landed clusters adsorb molecularly on the gold surface. We have also confirmed that the fragments of V(benzene)$_2$, i.e., benzene and V(benzene)$_1$, which are produced in the landing process, desorb from the gold substrate well below 180 K. Thus, such a recombination process is ruled out in the present second-order desorption kinetics. Another plausible origin of the second-order kinetics of adsorbates is their surface diffusion, which can produce a long tail in the high-temperature side of the TPD peaks.[49] For example, Vogt et al. reported that the TPD spectra for alcohol molecules adsorbed on SAMs display a second-order desorption (or symmetric) profile due to their diffusion on the SAM surfaces.[56] It is conceivable that the surface diffusion of the clusters leads to a random orientation in the desorption process and that the IRAS spectra for the V(benzene)$_2$/gold represent the random orientation of the clusters at any surface temperature.

Both the IRAS and TPD results demonstrate that the adsorption regime of the V(benzene)$_2$ clusters on the SAMs is very different from that on the bare gold surface; namely, a highly oriented geometry as well as higher thermal stability (i.e. larger adsorption heats) was obtained for the clusters supported on the SAM substrates. These results suggest that some significant physical effects at play in V(benzene)$_2$ adsorption on the SAM substrates. As mentioned in section 3.3, the analysis of the IRAS spectra shows that the V(benzene)$_2$ clusters are trapped with large orientation angles of $\Theta = 70-80°$ on the C_{18}-, and C_{22}-SAM substrates. When the V(benzene)$_2$ clusters are adsorbed on the outermost methyl groups of the alkanethiolate-SAMs, the clusters may prefer the adsorption geometry in which their molecular axes are perpendicular to the surface ($\Theta = \sim 0°$), because such geometry effectively involves an attractive CH$-\pi$ interaction between one of the capping benzene rings of the cluster and the outermost methyl groups. However, if the V(benzene)$_2$ clusters are incorporated in the SAM matrix, the clusters should interact with the hydrogen atoms of the lateral methylene groups of the surrounding alkanethiolate molecules. In this case, the molecular axis of the V(benzene)$_2$ molecules may be tilted considerably off the surface normal because of the methylene CH$-$benzene π interaction. Hence, the large orientation angles ($\Theta = 70-80°$) obtained herein suggest cluster penetration into the SAMs.

The TPD results for the V(benzene)$_2$/C_n-SAMs are also consistent with the cluster-penetration model. While second-order desorption kinetics were observed for the gold surface, the clusters supported on the long-chain C_n-SAMs with $n \geq 16$ display first-order desorption kinetics. They do so because the thermal desorption of the clusters trapped inside the long-chain SAMs can be regarded as a one-way diffusion into the SAM matrix. Such thermal desorption produces the following first-order desorption rate equation:[57]

$$-\frac{d\theta}{dt} = \upsilon_D \theta \exp(-E_D/RT) = k_D \theta \qquad (4)$$

Here υ_D is the preexponential factor and E_D is the activation energy for escaping from the inside of the SAM. Note that E_D corresponds to the adsorption heat (E_d) of the clusters soft-landed onto the C_n-SAM substrates.

It should be emphasized that the analysis of the TPD results in Figure 10 shows that the adsorption heat (E_d) of the clusters linearly increases against the chain length of the SAM, with an incremental E_d value/methylene unit of $\sim$4.5 kJ/mol. In this study, since the incident energy of the incoming clusters (i.e. $\sim$20 eV) is much larger than the observed adsorption heats (E_d $\sim$ 1 eV), it would allow the cluster ions to penetrate deeply into each SAM matrix. Such deep penetration into the SAM should provide a linear increment in the desorption activation energy, because the diffusion length for the desorption of the cluster increases as the chain length of the SAM grows. In the cluster-penetration process, furthermore, the incoming clusters presumably undergo multiple collisions with the alkanethiolate molecules. The multiple collisions would create a high soft-landing efficiency, because they could efficiently dissipate the cluster incident energy into numerous degrees of freedoms of the alkanethiolate-SAM and lead to a rapid thermalization.[33−35] Indeed, a large number of the deposited clusters can be kept intact in the SAM matrix even though the cluster incident energy of $\sim$20 eV is much larger than the binding energy of the V^+ and the two benzene molecules of the V(benzene)$_2^+$ (i.e. $\sim$5 eV).[3,4]

The kinetic energy distribution of the incident V(benzene)$_2$ cluster was estimated to be $\sim$20 eV at full-width half-maximum (fwhm) in this study. Thus, a small amount of the clusters deposited with low kinetic energy ($<$1 eV) might possibly land right on the methyl surface of the SAM matrix, being weakly physisorped *on* the methyl surface. However, we observed only one peak in the TPD spectra as well as a progressive shift to higher desorption temperature with the chain length, indicating that there was mainly one desorption state for the SAM-trapped clusters. Therefore, we could evaluate that the quantity of the clusters physisorbed on the methyl surface of the SAM matrix was negligible.

Like the desorption process from the long-chain C_{16-22}-SAMs, that of the clusters incorporated in the short-chain C_8- and C_{12}-SAMs is also expected to exhibit first-order desorption kinetics. However, the TPD spectra for the short-chain SAMs did not follow the Arrhenius equation, exhibiting nonlinear desorption kinetics. This unusual desorption kinetics may originate in the reduced rigidity of the shorter chain SAMs. For the long-chain SAM, as is well-known, a strong lateral van der Waals interaction between the alkanethiolates on the gold surface results in the "rigid" crystalline-phase SAM. However, the magnitude of the interaction decreases as the chain length shortens, so that the short-chain SAMs become less rigid.[58,59] As shown in Figure 6, the average orientation angle of the clusters penetrated in the C_{18}-SAM is not influenced by the substrate temperature, pointing to the immobility of the clusters trapped in the "rigid" long-chain SAM. In contrast, an orientation angle fluctuation, which exceeds the experimental uncertainty, was identified for the short-chain C_8-SAM. This result probably implies a relatively high mobility for the clusters trapped in the short-chain SAM, which could be caused by the fluxional behavior of the "less rigid" SAM produced as the substrate temperature rises. The thermal desorption from the less rigid matrix might not obey the simple desorption model of the Arrhenius equation, and might result in the nonlinear desorption kinetics.

The temperature dependence of the IRAS spectrum for the V(benzene)$_2$/C_{18}-SAM (see Figure 5b) shows that the IR peaks due to the V(benzene)$_2$ clusters remain in the IRAS spectrum

around room temperature, a finding which can be now ascribed to the large adsorption heat (>1 eV) of the SAM-incorporated V(benzene)$_2$ clusters. In general, such a large adsorption heat is limited to chemisorbed adsorbates. However, this study demonstrates that the V(benzene)$_2$ clusters can be trapped *physically* in the void spaces among the encompassing alkyl chains of the SAM, yielding an unusually large adsorption heat which is comparable to or greater than the adsorption heat of chemisorptions. This novel physisorption state, furthermore, can keep the supported clusters largely intact in the SAM matrix, while chemisorptions usually are accompanied by structural strains or dissociations of the adsorbates due to the strong chemical perturbation generated by the surface.

5. Conclusion

V(benzene)$_2$ cluster cations produced in the gas phase have been soft-landed onto a bare gold surface and various chain-length C_8- to C_{22}-SAMs of *n*-alkanethiols. The C_n-SAM species is found to serve as an excellent inert buffer matrix to discourage the decomposition of the neutralized V(benzene)$_2$ cluster in a soft-landing process, similar to a rare gas matrix. The high incident energy of 20 eV in the soft-landing process results in the penetration of the clusters into the C_n-SAM matrix. The incorporated clusters are highly oriented with their molecular axis canted 70−80° off the surface normal, a phenomenon which is probably due to the attractive CH−π interaction between the capping benzene rings of the cluster and the lateral methylene groups of the alkanethiolates. In addition, the adsorption heat of the clusters penetrating into the C_n-SAM increases with the chain length of the SAM. The V(benzene)$_2$ clusters penetrating into the long-chain SAMs possess unusually large adsorption heats, comparable to a typical adsorption heat of chemisorption, so that the thermal desorption of the clusters is suppressed, even at room temperature. In such a chemically unperturbed adsorption regime, the V(benzene)$_2$ clusters can retain the native 1D sandwich conformation; thus, it can be anticipated that they largely keep their intrinsic electronic and ferromagnetic properties in the SAM matrix.

The successful room-temperature isolation of gas-phase clusters in this study provides an advance that opens up a new opportunity to study various properties of the cluster-based materials by combining conventional surface science techniques. Furthermore, controlling the orientation of the anisotropic 1D sandwich clusters by means of the SAM matrix presented here illustrates that an understanding of the issues pertaining to the interactions between the deposited clusters and the support substrate will facilitate a fine-tuning of the cluster functionality on the substrate.

Acknowledgment. We are grateful to Prof. H. Onishi (Kobe University) for his suggestion regarding a TPD experimental setup. This work is partly supported by the 21st Century COE program "KEIO LCC" from the Ministry of Education, Culture, Sports, Science, and Technology (MEXT) and by a grant-in-aid for scientific research (C) (No. 15550129) from MEXT.

References and Notes

(1) Hoshino, K.; Kurikawa, T.; Takeda, H.; Nakajima, A.; Kaya, K. *J. Phys. Chem.* **1995**, *99*, 3035−3055.
(2) Nakajima, A.; Kaya, K. *J. Phys. Chem. A* **2000**, *104*, 176−191.
(3) Meyer, F.; Khan, F. A.; Armentrout, P. B. *J. Am. Chem. Soc.* **1995**, *117*, 9740−9748.
(4) Weis, P.; Kemper, P. R.; Bowers, M. T. *J. Phys. Chem. A* **1997**, *101*, 8207−8213.
(5) van Heijnsbergen, D.; von Helden, G.; Meijer, G.; Maitre, P.; Duncan, M. A. *J. Am. Chem. Soc.* **2002**, *124*, 1562−1563.
(6) Jaeger, T. D.; van Heijnsbergen, D.; Klippenstein, S. J.; von Helden, G.; Meijer, G.; Duncan, M. A. *J. Am. Chem. Soc.* **2004**, *126*, 10981−10991.
(7) Jaeger, T. D.; Pillai, E. D.; Duncan, M. A. *J. Phys. Chem. A* **2004**, *108*, 6605−6610.
(8) Lyon, J. T.; Andrews, L. *J. Phys. Chem. A* **2005**, *109*, 431−440.
(9) Wang, J.; Jellinek, J. *J. Phys. Chem. A* **2005**, *109*, 10180−10182.
(10) Yasuike, T.; Yabushita, S. *J. Phys. Chem. A* **1999**, *103*, 4533−4542.
(11) Pendy, R.; Rao, B. K.; Jena, P.; Blanco, M. A. *J. Am. Chem. Soc.* **2001**, *123*, 3799−3808.
(12) Kandalam, A. K.; Rao, B. K.; Jena, P.; Pandey, R. *J. Chem. Phys.* **2004**, *120*, 10414−10422.
(13) Miyajima, K.; Nakajima. A.; Yabushita, S.; Knickelbein, M. B.; Kaya, K. *J. Am. Chem. Soc.* **2004**, *126*, 13202.
(14) Wang, J.; Acioli, P. H.; Jellinek, J. *J. Am. Chem. Soc.* **2005**, *127*, 2812−2813.
(15) Heiz, U.; Schneider, W.-D. *J. Phys. D* **2000**, *33*, R85−R102.
(16) Heiz, U.; Bullock, E. L. *J. Mater. Chem.* **2004**, *14*, 564−577.
(17) Yoon, B.; Häkkinen, H.; Landman, U.; Wörz, A. S.; Antonietti, J.-M.; Abbet, S.; Judai, K.; Heiz, U. *Science* **2005**, *307*, 403−407.
(18) Dürr, H. A.; Dhesi, S. S.; Dudzik, E.; Knabben, D.; van der Laan, G.; Goedkoop, J. B.; Hillebrecht, F. U. *Phys. Rev. B* **1999**, *59*, R701−R704.
(19) Edmonds, K. W.; Binns, C.; Baker, S. H.; Maher, M. J.; Thornton, S. C.; Tjernberg, O.; Brookes, N. B. *J. Magn. Magn. Mater.* **2001**, *231*, 113−119.
(20) Moseler, M.; Häkkinen, H.; Landman, U. *Phys. Rev. Lett.* **2002**, *89*, 176103.
(21) Ouyang, Z.; Takáts, Z.; Blake, T. A.; Gologan, B.; Guymon, A. J.; Wisemen, J. M.; Oliver, J. C.; Davisson, V. J.; Cooks, R. G. *Science* **2003**, *301*, 1351−1354.
(22) Washburn, M. P. *Nat. Biol.* **2003**, *21*, 1156−1157.
(23) Gologan, B.; Takáts, Z.; Alvarez, J.; Wisemen, J. M.; Talaty, N.; Ouyang, Z.; Cooks, R. G. *J. Am. Soc. Mass Spectrom.* **2004**, *15*, 1874−1884.
(24) Judai, K.; Sara, K.; Amatsutsumi, S.; Yagi, K.; Yasuike, T.; Yabushita, S.; Nakajima, A.; Kaya, K. *Chem. Phys. Lett.* **2001**, *334*, 277−284.
(25) Cheng, H.-P. Landman, U. *Science* **1993**, *260*, 1304−1307.
(26) Bromann, K.; Felix, C.; Brune, H.; Harbich, W.; Monot, R.; Buttet, J.; Kern, K. *Science* **1996**, *274*, 956−958.
(27) Pugmire, D. L.; Woodbridge, C. M.; Boag, N. M.; Langell, M. A. *Surf. Sci.* **2001**, *472*, 155−171.
(28) Blass, P. M.; Akhter, S.; Seymour, C. M.; Lagowski, J. J.; White, J. M.; *Surf. Sci.* **1989**, *217*, 85−102.
(29) Welipitiya, D.; Dowben, P. A.; Zhang, J.; Pai, W. W.; Wendelken, J. F. *Surf. Sci.* **1996**, *367*, 20−32.
(30) Miller, S. A.; Luo, H.; Pachuta, S. J.; Cooks, R. G. *Science* **1997**, *275*, 1447−1450.
(31) Luo, H.; Miller, S. A.; Cooks, R. G.; Pachuta, S. J. *Int. J. Mass Spectrom. Ion Process.* **1998**, *174*, 193-217.
(32) Gologan, B.; Green, J. R.; Alvarez, J.; Laskin, J.; Cooks, R. G. *Phys. Chem. Chem. Phys.* **2005**, *7*, 1490−1500.
(33) Day, B. S.; Shuler, S. F.; Ducre, A.; Morris, J. R. *J. Chem. Phys.* **2003**, *119*, 8084−8096.
(34) Bosio, S. B. M.; Hase, W. L. *J. Chem. Phys.* **1997**, *107*, 9677−9686.
(35) Yan, T.; Isa, N.; Gibson, K. D.; Sibener, S. J.; Hase, W. L. *J. Phys. Chem. A* **2003**, *107*, 10600−10607.
(36) Mitsui, M.; Nagaoka, S.; Matsumoto, T.; Nakajima, A. *J. Phys. Chem. B* **2006**, *110*, 2968−2978.
(37) Schreiber, F. *Prog. Surf. Sci.* **2000**, *65*, 151−256.
(38) Love, J. C.; Estroff, L. A.; Kriebel, J. K.; Nuzzo, R. G.; Whitesides, G. M. *Chem. Rev.* **2005**, *105*, 1103−1169.
(39) Dubois, L. H.; Zegarski, B. R.; Nuzzo, R. G. *J. Am. Chem. Soc.* **1990**, *112*, 570−579.
(40) Linford, M. R.; Fenter, P.; Eisenberger, P. M.; Chidsey, C. E. D. *J. Am. Chem. Soc.* **1995**, *117*, 3145−3155.
(41) Porter, M. D.; Bright, T. B.; Allara, D. L.; Chidsey, C. E. D. *J. Am. Chem. Soc.* **1987**, *109*, 3559−3568.
(42) Rodriguez, K. R.; Shah, S.; Williams, S. M.; Teeters-Kennedy, S.; Coe, J. V. *J. Chem. Phys.* **2004**, *121*, 8671−8675.
(43) Hill, I. R.; Levin, I. W. *J. Phys. Chem.* **1979**, *70*, 842−851.
(44) McPhail, R. A.; Snyder, R. G.; Strauss, H. L.; Ellinger, C. A. *J. Phys. Chem.* **1984**, *88*, 334−341.
(45) Andrew, M. P.; Mattar, S. M.; Ozin, G. A. *J. Phys. Chem.* **1986**, *90*, 744−753.
(46) Hayden, B. E. In *Vibrational Spectroscopy of Molecules on Surface*; Yates, J. T., Jr., Modey, T. E., Eds.; Method of Surface Characterization; Plenum Press: New York, 1987; Vol. 1, Chapter 7.
(47) Debe, M. K. *J. Appl. Phys.* **1984**, *55*, 3354−3366.
(48) Parker, D. H.; Jones, M. E.; Koel, B. E. *Surf. Sci.* **1990**, *233*, 65−74.

(49) Kislyuk, M. U.; Rozanov, V. V. *Kinet. Catal.* **1995**, *36*, 80−88.
(50) King, D. A. *Surf. Sci.* **1975**, *47*, 384−402.
(51) Miller, J. B.; Siddiqui, H. R.; Gates, S. M.; Russell, J. N., Jr.; Yates, J. T., Jr.; Tully, J. C.; Cardillo, M. J. *J. Chem. Phys.* **1987**, *87*, 6725−6732.
(52) Rakov, V. S.; Denisov, E. V.; Laskin, J.; Futrell, J. H. *J. Phys. Chem. A* **2002**, *106*, 2781−2788.
(53) Syomin, D.; Kim, J.; Koel, B. E.; Ellison, G. B. *J. Phys. Chem. B* **2001**, *105*, 8387−8394.
(54) Hofmann, F.; Toennies, J. P. *Chem. Rev.* **1996**, *96*, 1307−1326.
(55) Barth, J. V. *Surf. Sci. Rep.* **2000**, *40*, 75−149.
(56) Vogt, A. D.; Beebe, T. P., Jr. *J. Phys. Chem. B* **1999**, 103, 8482−8489.
(57) Nagaoka, S.; Okada, E.; Doi, S.; Mitsui, M.; Nakajima, A. *Eur. Phys. J. D* **2005**, *34*, 239−242.
(58) Poirier, G. E.; Tarlov, M. J.; Rushmeier, H. E. *Langmuir* **1994**, *10*, 3383−3386.
(59) Fenter, P.; Eberhardt, A.; Liang, K. S.; Eisenberger, P. *J. Chem. Phys.* **1997**, *106*, 1600−1608.